Morphological stability of nanostructures

M. V. Ramana Murty*
Department of Physics and Cornell Center for Materials Research, Cornell University, Ithaca, New York 14853
(Received 24 August 2000)

Surface diffusion-induced smoothing of features below the roughening temperature is discussed using kinetic Monte Carlo simulations and a continuum description is developed. Rounding off the cusp in the surface free energy at low Miller index orientations permits a numerical solution of relaxation driven by surface diffusion. For both unidirectional and bidirectional sinusoidal profiles of wavelength L, the amplitude decays linearly with time and the decay time scales as L^{-3}. Surface morphology evolution below the roughening temperature as described by the continuum equation and a step model are compared.

I. INTRODUCTION

The fabrication of nanostructures by patterning and by various self-assembly techniques has received a lot of attention recently due to the unique size-dependent properties exhibited by the features. The small size of the features implies short thermal processing times for the fabrication of devices. Nanoscale features will smooth out rapidly by surface diffusion upon annealing to minimize the surface free energy.[1–3] Therefore, it is of interest to determine how the rate of decay scales with feature size.

A continuum description of surface diffusion mediated relaxation was derived by Herring[4] and further developed by Mullins.[5] The theory can be readily applied to amorphous materials and to single-crystal surfaces above their roughening temperature T_R. However, as noted by Mullins,[5] a direct application of the theory to crystalline materials below T_R is prevented by the presence of a cusp in the surface free energy at low Miller index orientations.

To get around the nonanalyticity of the free energy, step models[6] involving rate equations for individual steps have been developed to describe the smoothing of a rough surface.[7–10] A continuum approach has also been developed that involves the explicit identification of facet boundaries.[11–13] However, these methods become complicated when the surface geometry is not simple, i.e., does not possess symmetry. In addition, these methods[7,8,11–15] and related Monte Carlo simulations[16–19] have led to widely different predictions for the temporal evolution, the wavelength scaling exponent, and the shape of a sinusoidal profile during decay.

In this paper, surface diffusion mediated relaxation below T_R is discussed with the aid of kinetic Monte Carlo simulations and a continuum description is developed. The nonanalytic point in the free energy is removed by rounding off a small section through the cusp. The resulting nonlinear equation describes surface dynamics in systems where the detachment and diffusion of atoms across a terrace is the rate-determining process. The method can be applied to materials whose equilibrium crystal shape consists of the curved region meeting the facet without a discontinuity in slope. The description of surface morphology evolution according to the continuum equation and the step model is compared.

The method of rounding off the cusp in the projected surface free energy has been suggested previously.[14] However, this approach to surface relaxation has been challenged by Rettori and Villain,[7] and subsequently by the authors who proposed it originally.[15] The various issues associated with this approach are addressed below.

The paper is organized as follows. Kinetic Monte Carlo simulations are discussed in Sec. II. The continuum method is developed and applied to sinusoidal and patterned surfaces in Sec. III. Limitations of the continuum approach are discussed in Sec. IV, followed by a conclusion in Sec. V.

II. KINETIC MONTE CARLO SIMULATIONS

Important aspects of the decay process can be highlighted using a Monte Carlo simulation. We use a solid-on-solid model with a square lattice. The energy of an atom with p nearest neighbors is $-p\varepsilon$. Atoms are only allowed to hop to nearest-neighbor sites. The hopping rate f from site i to site j is

$$f=\begin{cases}\nu\exp[-(E_j-E_i+\varepsilon_d)/k_BT], & E_i<E_j\\ \nu\exp[-\varepsilon_d/k_BT], & E_i\geqslant E_j.\end{cases} \tag{1}$$

Here, ν is the attempt frequency, k_B is the Boltzmann constant, and T is the temperature. The adatom (and vacancy) diffusion barrier on the terrace is ε_d. The parameter values chosen for the simulations are $\nu=10^{12}$ s^{-1}, $\varepsilon_d=0.3$ eV, and $\varepsilon=0.3$ eV. The roughening temperature for the (001) facet is $T_R=0.62\varepsilon/k_B$.[20] There is no Ehrlich-Schwoebel barrier and we expect diffusion-limited kinetics. Kinetic Monte Carlo simulations for this model have been reported before.[16,18] Here, I only elaborate on aspects not discussed previously.

Consider the decay of bidirectional sinusoidal profiles of the form

$$z(x,y)=z_0\cos\left(\frac{2\pi x}{L}\right)\cos\left(\frac{2\pi y}{L}\right). \tag{2}$$

A discretized version of Eq. (2) is set up and we follow the evolution of the surface. Figure 1 shows snapshots of the surface at different stages of decay for a profile with initial amplitude $z_0=4$ and wavelength $L=120$. Time is measured in units of $[\nu\exp(-\varepsilon_d/k_BT)]^{-1}$. The temperature for the simulation $T=0.33\varepsilon/k_B=0.54T_R$ is well below the roughening temperature. The simulations were performed on a 240 $\times$240 cell with periodic boundary conditions. The sinusoidal

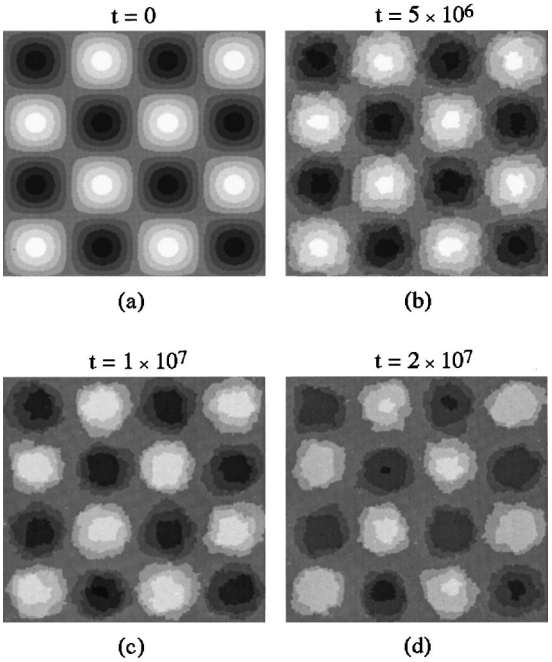

FIG. 1. Snapshots of the surface morphology during the evolution a bidirectional sinusoidal profile of wavelength $L=120$ and initial amplitude $z_0=4$. The unit of time is $[\nu \exp(-\varepsilon_d/k_BT)]^{-1}$. Lighter regions represent higher points on the surface.

shape is not preserved during decay as the regions near the extrema and the saddle points get flattened. This has been observed in experiments[21] and occurs due to the lower free energy of the facet compared to neighboring orientations.

Figure 2 shows the evolution of the Fourier amplitude[22] $|Z(\mathbf{q},t)|, \mathbf{q}=(2\pi/L, 2\pi/L)$ for wavelengths from $L=16$ to $L=160$ as a function of scaled time t/L^3. The initial amplitude $z_0=4$ for all wavelengths and the temperature $T=0.54T_R$. The results represent an average over at least $16(L\times L)$ cells at each wavelength. We observe that there is no unique wavelength scaling exponent. However, for long wavelengths the decay can be described approximately by

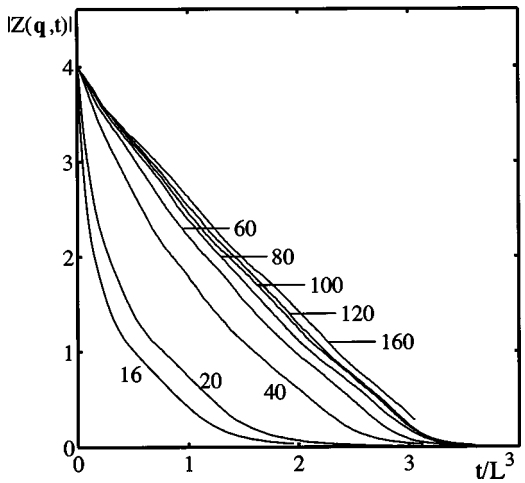

FIG. 2. Decay of the Fourier amplitude $|Z(\mathbf{q},t)|$ at $\mathbf{q}=(2\pi/L, 2\pi/L)$ for bidirectional sinusoidal profiles of wavelengths $L=16$ to $L=160$. Due to the use of discretized sinusoidal profiles the starting amplitude was slightly different from four for each wavelength, and was normalized to four for this figure.

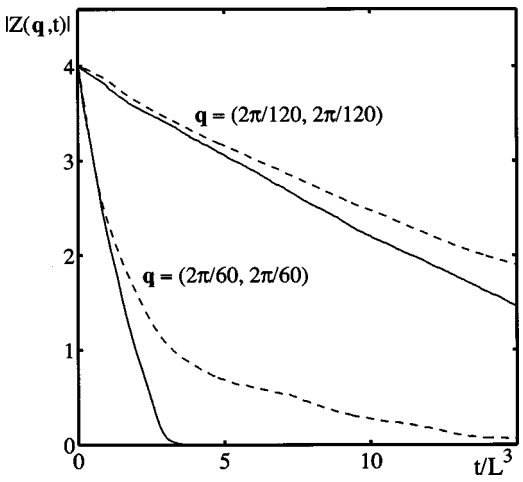

FIG. 3. Comparison of the evolution of the Fourier amplitude for two superposed wave vectors $\mathbf{q}=(2\pi/L, 2\pi/L)$, $L=60$ and 120 (dashed lines) with the situation when only one wave vector is present (solid lines). The data is averaged over 10 simulations, each on a 240×240 cell.

$$|Z(\mathbf{q},t)| \approx z_0 - \beta t/L^3. \tag{3}$$

The wavelength scaling exponent of $n\approx3$ is in agreement with a step model due to Rettori and Villain.[7] It is noted that for the very short wavelengths ($L=16,20$), $n\approx5$ gives a better fit and there is a gradual transition from $n\approx5$ to $n\approx3$.

Consider now the decay of two superposed bidirectional sinusoidal profiles of the form in Eq. (2). On a (240×240) cell, bidirectional profiles with wavelengths $L=60$ and 120 and initial amplitude $z_0=4$ are superposed and we follow the evolution at $T=0.54T_R$. The evolution of Fourier amplitudes for the superposed wavelengths is compared to the decay when only one wavelength is present in Fig. 3. The decay is clearly different in the two situations. Surface diffusion-mediated relaxation below the roughening temperature must therefore be described by a nonlinear equation.[8] This is in contrast to the situation above T_R where the Herring-Mullins equation, a linear equation, describes surface diffusion-mediated relaxation.[23]

III. A CONTINUUM DESCRIPTION

The description of facets and the decay process below T_R presents no conceptual difficulty in the Monte Carlo simulations. However, these simulations are extremely slow. For example, the decay process in Fig. 1 required on the order of 10^{12} atom jumps. The high wavelength scaling exponent implies that the time required for simulations goes up very rapidly with increasing wavelength. A continuum description of the decay process can overcome this limitation.

Below T_R, the projected [onto the (001) plane] surface free energy per unit area G has the general form[24]

$$G = G_0 + G_1(z_x^2+z_y^2)^{1/2} + \frac{1}{3}G_3(z_x^2+z_y^2)^{3/2}. \tag{4}$$

Here, $z(x,y)$ is the height at position (x,y) and $(z_x,z_y) \equiv \nabla z$. The three terms in the summation represent, per unit area, the terrace free energy (G_0), the step free energy (G_1

term) and the step-step interaction energy (G_3 term). For simplicity, G_1 and G_3 are taken to be independent of the azimuth.

Mass transport occurs from regions of high chemical potential to regions of low chemical potential. The chemical potential μ [in excess of an infinitely flat (001) plane] is given by[4,5]

$$\mu = -\Omega\left[\frac{\partial}{\partial x}\left(\frac{\partial G}{\partial z_x}\right)+\frac{\partial}{\partial y}\left(\frac{\partial G}{\partial z_y}\right)\right] \tag{5}$$

where Ω is the atomic volume.

For a circular island of radius r, Eq. (5) gives (for $G_3=0$) $\mu=\Omega G_1/r$, the expected Gibbs-Thompson relation.[25] At places where $\nabla z=0$, Eq. (5) has the form $\mu=0\cdot\infty$ creating a difficulty for an analytical or numerical solution. Of course, μ is finite at all points on the surface and due to adatoms and vacancies on facets.[7]

We can get around the uncertainty in μ at $\nabla z=0$ by replacing $(z_x^2+z_y^2)$ in Eq. (4) with $(z_x^2+z_y^2+\alpha^2)$. The parameter α has the units of slope and is chosen to be sufficiently small as discussed below. Rounding off the cusp permits[14,26] the evaluation of μ at all orientations, including $\nabla z=0$.

A. Equilibrium crystal shape

We first show that one approaches the exact equilibrium shape of the crystal and the exact value of μ in the limit $\alpha\to 0$. Consider a crystal of a fixed volume V placed on a substrate with the constraint that the angle of contact $\theta=45°$. (As long as $\tan\theta \gg \alpha$, the conclusion remains unchanged.) The equilibrium shape of the crystal $z\equiv f(r)$ with $r=(x^2+y^2)^{1/2}$ is given by the Landau-Andreev construction[24,27]

$$\frac{\mu(\alpha)}{2\Omega}r = G_1 f_r (f_r^2+\alpha^2)^{-1/2} + G_3 f_r (f_r^2+\alpha^2)^{1/2}, \tag{6}$$

where $f_r \equiv df/dr$. Figure 4(a) shows the equilibrium shape of the crystal for three different values of $\alpha=0.001$, 0.01, and 0.1, as well as the exact shape with $\alpha=0$ for the ratio $G_3/G_1=0.1$. For finite values of α, the equilibrium shape approaches the exact shape as $\alpha\to 0$. Figure 4(b) shows the chemical potential for several values of α and three different values of the ratio G_3/G_1. As $\alpha\to 0$, μ approaches the exact value. Note that $\mu=2G_1\Omega/r^*$, r^* being the radius of the facet, with contributions from both the step free energy and the step-step interaction energy terms.

As mentioned above, one encounters $\mu=0\cdot\infty$ on the (001) plane when using Eq. (5). By rounding off the cusp we get

$$\mu(\alpha) = -\Omega\left(\frac{G_1}{\alpha}+G_3\alpha\right)(z_{xx}+z_{yy}). \tag{7}$$

While it is true that one replaces the ∞ by a finite number $(=G_1/\alpha+G_3\alpha)$, it is also the case that the 0 is replaced by a finite number $(=z_{xx}+z_{yy})$. In other words, there is no true facet when the cusp is removed from the projected surface free energy. The region with the (001) orientation has a small curvature. In the limit $\alpha\to 0$, $\mu(\alpha)$ approaches the exact value. While a particular functional form was chosen for rounding off the cusp, it is evident from both the geometrical (Wulff) and the analytical (Landau-Andreev) construction of the equilibrium crystal shape[24] that any reasonable function would yield the same result.

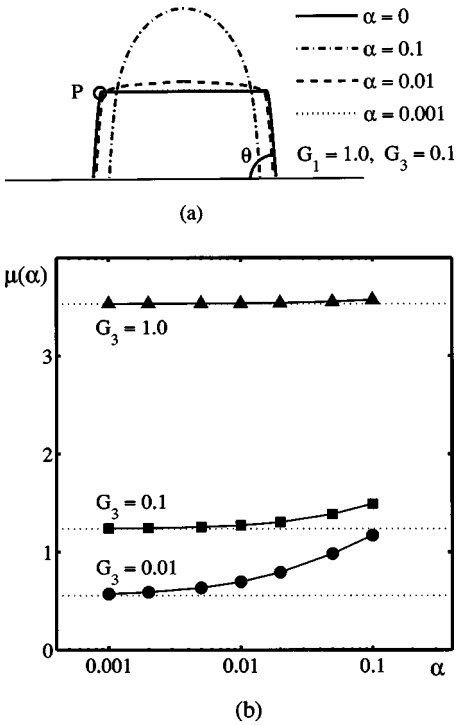

FIG. 4. (a) Equilibrium shape of the crystal according to Eq. (6) for a fixed volume $V=1$, $G_3=0.1$, $G_1=1$, and $\alpha=0$, 0.001, 0.01, and 0.1. The constraint of $\theta=45°$ contact angle was imposed in calculating the equilibrium shape. Note that the scale along horizontal and vertical directions is different. The equilibrium shape approaches the exact shape ($\alpha=0$) as $\alpha\to 0$. (b) Chemical potential on the surface as a function of α for $G_1=1$ and three different values of $G_3=0.01$, 0.1, and 1. The dotted line is the exact chemical potential calculated with $\alpha=0$. As $\alpha\to 0$, the chemical potential approaches the exact value in all three cases.

B. Equation for surface diffusion-mediated relaxation

We now consider surface morphology evolution under nonequilibrium conditions. In such situations, one defines a local chemical potential according to Eq. (5). The surface current $\mathbf{j}$ is taken as

$$\mathbf{j} = -\frac{D_s}{k_B T} c_{\mathrm{eq}} \nabla\mu. \tag{8}$$

where D_s is the adatom diffusivity, c_{eq} is the equilibrium adatom concentration [on an infinitely large (001) plane], k_{B} is the Boltzmann constant, and T is the temperature.[5] Conservation of mass gives

$$\frac{\partial z}{\partial t} = -\Omega\nabla\cdot\mathbf{j} = \kappa\nabla^2\mu \tag{9}$$

where the coefficient $\kappa = D_s c_{eq}\Omega/k_{\mathrm{B}}T$. The expression for surface current, Eq. (8), corresponds to diffusion-limited transport, where adatoms do not face Ehrlich-Schwoebel barriers at step edges.[7,8] We are assuming that transport is slow with respect to one variable, namely, the mean step position, and extremely fast for all other variables. Surface morphol-

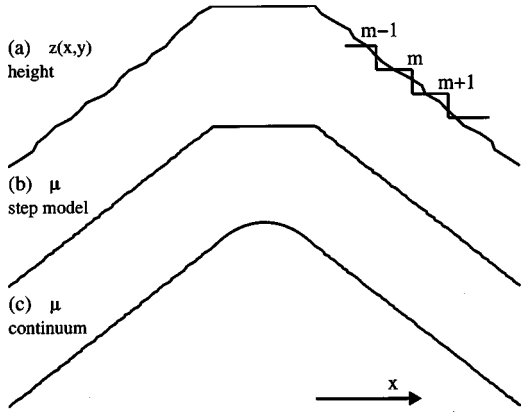

FIG. 5. Surface morphology evolution according to the continuum equation and the step model. (a) Schematic of the surface. Chemical potential variation across the *average surface* according to (b) The step model. (c) The continuum equation.

ogy evolution is described in the limit where step fluctuations get established quickly, and adatom concentration on the terraces comes to local equilibrium with the steps quickly.

C. Connection with the step model

The equation for annealing, Eq. (9), was written using the standard principles of irreversible thermodynamics. Away from the facets, the equation can be obtained from a step model. The following derivation closely follows the work of Ozdemir and Zangwill.[8] We assume that adatoms are the only diffusing species.

Consider the surface $z(x,y)$ shown in Fig. 5(a). At the microscopic level, it is composed of steps and terraces. Consider the section with steps labeled $m-1$, m, and $m+1$. The terrace between steps m and $m+1$ is referred to as the mth terrace. The position of step m is x_m and its velocity is

$$\frac{dx_m}{dt}=-\Omega\left(k_+\frac{\delta F^+}{\delta x_m}+k_-\frac{\delta F^-}{\delta x_m}\right). \tag{10}$$

Here, δF^+ (δF^-) is the change in the free energy when nearby atoms on the lower (upper) terrace are transferred to the step edge, and k_+ and k_- are kinetic coefficients. The change in free energy when atoms from the lower terrace are transferred to the step edge is

$$\delta F^+=[\mu_m-\overline{\mu}_m(x_m^+)]\frac{\delta x_m}{\Omega}. \tag{11}$$

Here, μ_m is the chemical potential of an atom attached to step m, and $\overline{\mu}_m$ is the chemical potential of adatoms on the mth terrace. The positions x_m^+ and x_m^- are adjacent to step m on the lower and upper side, respectively. Combining Eqs. (10) and (11), we get

$$\frac{dx_m}{dt}=-k_+[\mu_m-\overline{\mu}_m(x_m^+)]-k_-[\mu_m-\overline{\mu}_{m-1}(x_m^-)]. \tag{12}$$

For small deviations from equilibrium, the chemical potential of adatoms with density $c(x)$ is given by[5]

$$\overline{\mu}=k_BT\ln\left(1+\frac{c(x)-c_{eq}}{c_{eq}}\right)\approx k_BT\frac{c(x)-c_{eq}}{c_{eq}}. \tag{13}$$

We can also express the step velocity as

$$\frac{dx_m}{dt}=\overline{\nu}\left[D_s\frac{dc_m(x)}{dx}\bigg|_{x_m^+}-D_s\frac{dc_{m-1}(x)}{dx}\bigg|_{x_m^-}\right], \tag{14}$$

where $\overline{\nu}$ is the areal density of an adatom. The adatom density $c(x)$ can be determined for specific geometries from

$$\nabla^2c(x)=\frac{\partial c(x)}{\partial t}=0. \tag{15}$$

By setting the time derivative to zero, we are assuming slow moving steps and that the adatom density can quickly respond to the moving steps. For a circular stack of islands, the adatom density on the mth terrace is of the form

$$c_m(x)=a_m+b_m\ln x \tag{16}$$

and for straight steps

$$c_m(x)=a_m+b_mx. \tag{17}$$

The coefficients a_m and b_m are determined by applying appropriate boundary conditions. In the general case, using Eqs. (12), (13), and (14), we equate the components of the step velocity to get

$$v_m^+=\overline{\nu}D_s\frac{dc_m(x)}{dx}|_{x_m^+}=-k_+\left(+k_BT-\frac{k_BT}{c_{eq}}c_m(x_m^+)+\mu_m\right) \tag{18}$$

and

$$v_{m+1}^-=-\overline{\nu}D_s\frac{dc_m(x)}{dx}|_{x_{m+1}^-}=-k_-\left(+k_BT-\frac{k_BT}{c_{eq}}c(x_{m+1}^-)+\mu_{m+1}\right). \tag{19}$$

From Eqs. (18) and (19), we get

$$\overline{\nu}D_s\left[\frac{1}{k_+}\frac{dc_m(x)}{dx}\bigg|_{x_m^+}+\frac{1}{k_-}\frac{dc_m(x)}{dx}\bigg|_{x_{m+1}^-}\right]=(\mu_{m+1}-\mu_m)-\frac{k_BT}{c_{eq}}[c_m(x_{m+1}^-)-c_m(x_m^+)]. \tag{20}$$

For diffusion-limited kinetics, we ignore the term on the left-hand side of Eq. (20) to give[8]

$$\mu_{m+1}-\mu_m=\frac{k_BT}{c_{eq}}[c_m(x_{m+1}^-)-c_m(x_m^+)]. \tag{21}$$

To take the continuum limit, we recognize that the surface height $z(x,y)$ can be related to step velocity by

$$\frac{\partial z}{\partial t}=\nabla z\frac{dx_m}{dt}. \tag{22}$$

If the step height is a, we can write the slope $\nabla z=a/(x_{m+1}-x_m)$. From Eqs. (14) and (22), we get

$$\frac{\partial z}{\partial t} = \overline{\nu a} D_s \left[\frac{\left. \frac{dc_m(x)}{dx} \right|_{x_{m+1}^-} - \left. \frac{dc_m(x)}{dx} \right|_{x_m^+}}{x_{m+1} - x_m} \right]. \tag{23}$$

With Eq. (21) and setting $\overline{\nu a} = \Omega$, this becomes

$$\frac{\partial z}{\partial t} = \frac{D_s c_{\mathrm{eq}} \Omega}{k_{\mathrm{B}} T} \nabla^2 \mu, \tag{24}$$

which is the same as Eq. (9).

Away from the facets where $\nabla z \neq 0$, the step model and the continuum equation predict the same behavior. The description is, however, different on the plateaus where $\nabla z \approx 0$.

On a dynamically evolving surface, one sets the adatom density to be constant at the extrema in a step model.[7,8,10] For example, the coefficients b_m in Eqs. (16) and (17) are set equal to zero at the top of a circular stack of islands or straight steps. This implies that the chemical potential is constant at the extrema. The variation of chemical potential across the surface according to a step model is sketched in Fig. 5(b).

A solution using the continuum equation, Eq. (9), on the other hand, shows (see the example of bidirectional sinusoidal profile below) that the chemical potential varies everywhere including the plateaus. The variation of the chemical potential according to the continuum equation is sketched in Fig. 5(c).

Should the chemical potential vary on the plateaus? The answer to this question is determined by the nature of the fluctuations. Note that we are attempting to describe the evolution of *the average surface profile* with the continuum equation. The snapshots of the surface morphology in Fig. 1 give us a clue. Even though we start with perfect (discretized) sinusoidal profiles, the various hilltops and valleys follow different trajectories in phase space due to the random (Brownian) nature of the diffusion process. There is no unique facet radius and even the number of layers might be different at different hilltops (and valleys). Now the radius of the island bounding the facet decreases gradually during decay, typically following a power law (when averaged).[28] There is a finite probability for finding a facet of a particular radius all the way down to a single atom.[29] If we average the chemical potential across the surface for a large number of profiles such as Fig. 1, we should expect the chemical potential to vary smoothly across the plateaus of the average surface.

D. Bidirectional sinusoidal profiles

We now apply the equation of motion for annealing, Eq. (9), to describe bidirectional sinusoidal profile decay below T_{R}. The starting surface is given by Eq. (2) with initial amplitude $z_0 = 2$. The paramaters $G_1 = 0.1$, $G_3 = 0.01$, $\kappa = 1$, and $\alpha = 0.01$. The grid size is $\Delta x = \Delta y = L/50$. Figure 6(a) shows the decay of the amplitude A (defined as the local maximum) for three different wavelengths $L = 50$, 100, and 150. Following an initial transient, the amplitude decay can be expressed as

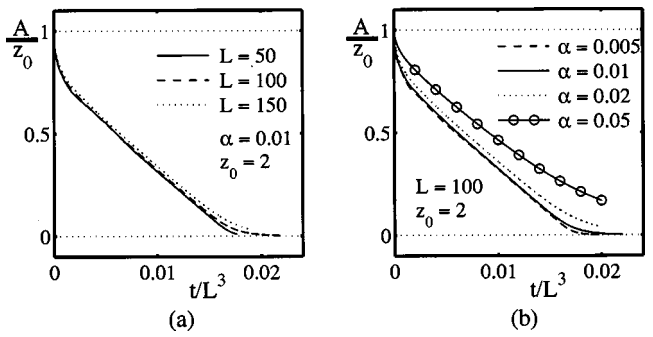

FIG. 6. The decay of the amplitude (defined as the local maximum in height) for bidirectional sinusoidal profiles for three different wavelengths. The initial amplitude $z_0 = 2$. The wavelength scaling exponent is $n \approx 3.0$. (b) The dependence of the amplitude decay on α for a fixed wavelength $L = 100$.

$$\frac{dA}{dt} \approx -\beta / L^n \tag{25}$$

with $n \approx 3.0$. Figure 6(b) shows the amplitude decay for the wavelength $L = 100$ with four different values of $\alpha = 0.005$, 0.01, 0.02, and 0.05. The rate of decay is found to be insensitive to the value of α and grid size (not shown), provided they are sufficiently small. The form of the amplitude evolution is in agreement with a previous analysis using rate equations for steps[7] and with Monte Carlo simulations at long wavelengths (Fig. 2).[16,17] The parameter $\beta = 92$ from the numerical solution is also in agreement with $\beta \approx 77$ from the step model.[7] The analytical estimate $\beta \approx 77$ takes into account an additional factor of 2 not included in the step model[7] since, as noted above, μ near the facet is closer to $2G_1\Omega/r^*$ rather than $G_1\Omega/r^*$.[30]

Figure 7 shows a section of the surface morphology through the extrema and variation of the chemical potential over the same region. The starting surface was a bidirectional sinusoidal profile of wavelength $L = 200$ and initial amplitude $z_0 = 4$. The sinusoidal shape is not preserved and flattened regions are observed at the extrema (and also saddle points, not shown). The regions with slope $|\nabla z| \ll \alpha$ may be regarded as a facet and the set of points with a kink in $|\nabla^2 z|$

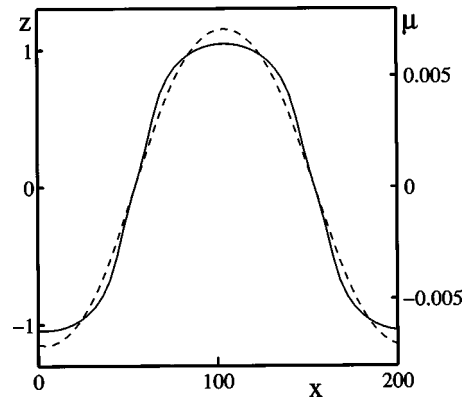

FIG. 7. The variation of surface height z (solid line) and the chemical potential μ (dashed line) for a bidirectional sinusoidal profile of wavelength $L = 200$. The $y = L/2$ section is shown at scaled time $t/L^3 = 6.25 \times 10^{-3}$. Note that the chemical potential varies smoothly everywhere, including the plateaus.

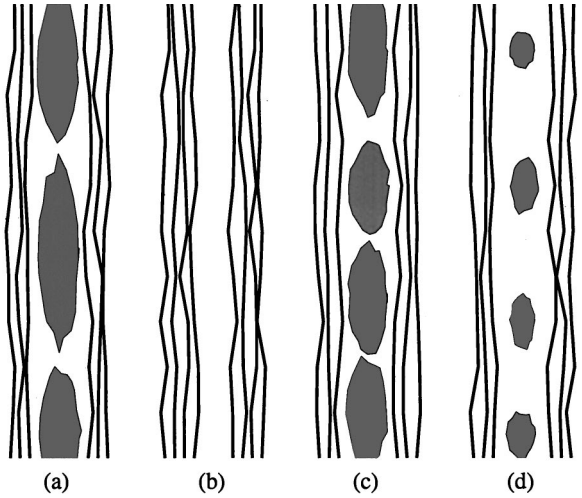

FIG. 8. (a) Schematic of the equilibrium surface morphology relevant to the unidirectional surface corrugations. Since steps are freely wandering, the opposite steps will cross several times along their length. (b)–(d) View near the maximum during the evolution of a unidirectional sinusoidal corrugation. The opposite steps at the extrema cross as they wander due to fluctuations. The 2D islands that form eventually decay away leading to the removal of one monolayer.

can be regarded as the operational definition of the facet boundary. As noted above, the chemical potential varies smoothly everywhere, including the plateaus.

E. Unidirectional sinusoidal profiles

Before applying Eq. (9) to unidirectional sinusoidal profiles, let us consider the equilibrium and nonequilibrium pictures in more detail. The equilibrium crystal shape appropriate to this geometry is calculated according to the Landau-Andreev construction[24,27] with the additional constraint $z_y = 0$. The condition of equilibrium implies that steps are freely wandering. Hence, as shown in Fig. 8(a), we expect opposite steps making the facet to have crossed several times along the length to form two-dimensional (2D) islands. Since the 2D islands necessarily have in-plane curvature, μ consists of contributions from both the step free-energy term (μ_1) and the step-step interaction energy term (μ_3).[34] In fact, $\mu = G_1\Omega/w$, $2w$ being the width of the facet.

As shown in Figs. 8(b)–8(d), the evolution of a unidirectional sinusoidal profile involves (i) building up fluctuations at the two opposite steps at the extrema leading to contact and formation of 2D islands, and (ii) the decay of the 2D islands.[7] The continuum method describes the evolution in the limit where process (i) occurs rapidly, and the decay of the 2D islands is the slow process.

Figure 9(a) shows the decay of the amplitude of a unidirectional sinusoidal profile $z(x,y) = z_0\cos(2\pi x/L)$ for three different wavelengths $L = 100$, 200, and 300. The parameters are $G_1 = 0.1$, $G_3 = 0.01$, $\kappa = 1$, and $\alpha = 0.01$. The initial amplitude is scaled with wavelength $z_0/L = 0.02$ and the grid size $\Delta x = \Delta y = L/100$. After the initial transient, the amplitude decay can be described by Eq. (25) with $n = 3.0$. The functional form of the amplitude decay agrees with a previous continuum description.[11–13] In addition, the parameter $\beta = 22$ from the numerical solution is also in good agreement

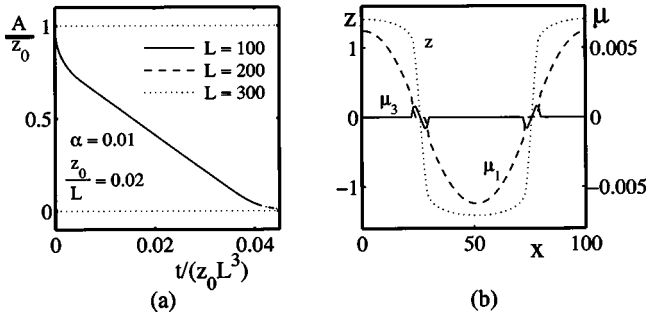

FIG. 9. (a) Amplitude decay of unidirectional sinusoidal profiles for three different wavelengths. The initial amplitude was scaled with the wavelength $z_0/L = 0.02$. The wavelength scaling exponent is $n = 3$. (d) Surface profile (z, dotted line) and the contributions of the step free energy (μ_1, dashed line) and the step-step interaction energy (μ_3, solid line) to the chemical potential.

with $\beta \approx 20$ from the previous description.[13] This is not surprising since these models[11–13] make the same assumptions as the one described here. However, the form of the amplitude decay disagrees with the wavelength scaling exponent of $n = 5$ in a step model[8] and in previous Monte Carlo simulations.[16]

The contribution of the step free-energy term to the chemical potential is not included in the step model.[8] Figure 9(b) shows the surface profile and the contributions μ_1 and μ_3 to the chemical potential for the wavelength $L = 100$ at $t/L^3 = 0.01$ according to the continuum description. The surface profile consists of plateaus near the maximum and minimum, as often observed in experiments.[31–33] In the curved regions $|\nabla z| \gg \alpha$, the dominant contribution to μ comes from μ_3 [μ_1 must strictly vanish according to Eqs. (4) and (5).[8]] On the plateaus $|\nabla z| \ll \alpha$, μ varies significantly and the dominant contribution to μ comes from μ_1. Physically, this corresponds to the presence of 2D islands. The Monte Carlo simulations in previous work[16] were limited to small wavelengths due to the long computation times involved. Just as for the bidirectional sinusoidal profiles (Sec. II), it is plausible that there is a transition to a linear decay of the amplitude with t/L^3 scaling at long wavelengths.

F. Patterned surfaces

Surface diffusion mediated relaxation is a slow process. The power-law scaling of the amplitude decay implies that one has to fabricate structures with nanoscale dimensions to determine scaling laws and activation energies. Given the difficulties in the fabrication of periodic profiles with nanometer scale features, the use of ''patterned'' surfaces for such purposes has become popular.[38–41] Such surfaces are generated by growth or ion bombardment and exhibit a characteristic length scale but always consist of a distribution of wavevectors.[34–37] Since the equation describing relaxation is non-linear, the results from such studies[38–41] are not representative of sinusoidal profile decay.

To illustrate this, we generate a ''patterned'' surface using a standard differential equation with a stochastic term.[42] Snapshots of the surface morphology during subsequent evolution as described by Eq. (9) are shown in Figs. 10(a) and 10(b). The parameters are $\kappa = 1$, $G_1 = 0.1$, $G_3 = 0.01$ and $\alpha = 0.01$ and the simulations were performed on a 200×200

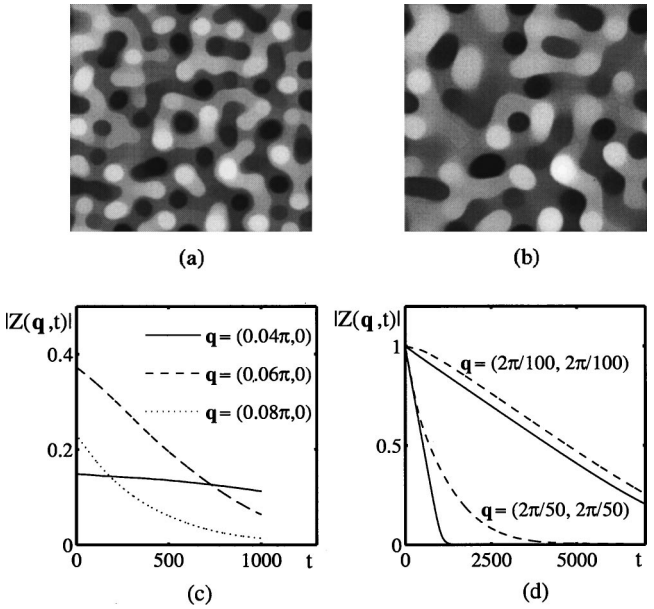

FIG. 10. Snapshots of the surface morphology during annealing of a patterned surface at times (a) $t=100$ and (b) $t=500$. (c) The evolution of three Fourier amplitudes. (d) Evolution of the Fourier amplitudes during the decay of two bidirectional sinusoidal profiles of wavelengths $L=50$ and 100 evolving separately (solid lines) and when superposed (dashed lines).

cell with $\Delta x=\Delta y=1$. The amplitudes of the longer wavevectors decay away faster than those of the shorter wave vectors, leading to a gradual increase in the characteristic length scale. Figure 10(c) shows the variation of the amplitudes of three wave vectors with time. Unlike sinusoidal profiles, the decay is not linear with time and there is no unique wavelength scaling exponent.

The nonlinear nature of the decay process is further illustrated in Fig. 10(d) using the example of two superposed bidirectional sinusoidal profiles of wavelengths $L=50$ and 100. The decay of the amplitudes corresponding to the two wave vectors for the superposed profiles is different from the situation where only one wave vector is present. The behavior is similar to that observed in kinetic Monte Carlo simulations (Fig. 3).

IV. DISCUSSION

In applying the equation for annealing, Eq. (9), we have made a number of simplifications. This includes diffusion-limited kinetics (no Ehrlich-Schwoebel barrier) and a surface free energy independent of azimuth. We also make the assumptions about slow moving steps and the quick establishment of step fluctuations. The rate determining process is taken to be the detachment and diffusion of atoms across a terrace. Furthermore, surface morphology evolution is only described for materials whose equilibrium crystal shape consists of the curved region meeting the facet without a discontinuity in slope.

In some situations, annealing may proceed through nucleation.[3] If at some place on the surface $\nabla z=0$ and $\nabla^2 z=0$, the chemical potential $\mu=0$. There is nothing unusual about $\mu=0$ since it refers to an excess chemical potential. However, such a location is a potential site for island nucleation. The surface kinetics will not be described accurately by Eq. (9) in this situation, since no nucleation mechanism is built into it.

From a practical standpoint, how small a value should one choose for α? As a general observation, α should be much smaller than the maximum slope on the surface. One should always try a few values of α to make sure that the results are insensitive to its value. As α is made smaller, one needs to use a finer grid (smaller Δx and Δy) to accurately calculate the chemical potential near the edge of the plateau [point P in Fig. 4(a)] where $\nabla^2 z$ diverges.

Finally, it was argued above that the step model does not give an accurate description of the chemical potential variation over the plateau for the average surface. Why do we get good agreement between the continuum equation and the step model for the decay of bidirectional sinusoidal profiles? In the step model one considers every position of the step during the decay of a single layer. Hence, the total decay time for an island may still be reasonably described in a step model.

On heuristic grounds, the chemical potential is expected to vary over the plateau for the average surface. We could speculate that in the limit $\alpha\rightarrow 0$, the chemical potential variation over the plateau represents the ensemble average. However, I do not have any proof of the above statement.

V. CONCLUSION

In conclusion, surface diffusion induced smoothing below the roughening temperature has been discussed using kinetic Monte Carlo simulations and a continuum equation. Rounding off the cusp in the surface free energy at low Miller index orientations permits a numerical solution of relaxation driven by surface diffusion. The continuum equation and its relation to the step model is discussed in detail.

ACKNOWLEDGMENTS

I gratefully acknowledge discussions with Barbara Cooper, Eugene Kolomeisky, Jim Sethna, and Chris Henley. I also thank Mike Aziz for providing a copy of their work (Ref. 41) prior to publication. Guy Jennings provided assistance with computers. This work began at Cornell University with support form the Cornell Center for Materials Research, which is funded by NSF under Award No. DMR-9632275, and made use of the resources of the Cornell Theory Center. The work continued at Argonne National laboratory with support from the US DOE, BES-DMS under Contract No. W-31-108-ENG-38.

*Present address: Materials Science Division, Argonne National Laboratory, Argonne, IL 60439. Email address: murty@anl.gov

[1] C.G. Zimmermann, M. Yeadon, K. Nordlund, J.M. Gibson, R.S. Averback, U. Herr, and K. Samwer, Phys. Rev. Lett. **83**, 1163 (1999).

[2] A. Ichimiya, K. Hayashi, E.D. Williams, T.L. Einstein, M. Uwaha, and K. Watanabe, Phys. Rev. Lett. **84**, 3662 (2000).

[3] N. Combe, P. Jensen, and A. Pimpinelli, Phys. Rev. Lett. **85**, 110 (2000).

[4] C. Herring, in *Structure and Properties of Solid Surfaces*, edited

by R. Gomer and C.S. Smith (Univ. Chicago Press, Chicago, 1 1952).
[5] W.W. Mullins, in *Metal Surfaces: Structure, Energetics and Kinetics*, edited by N.A. Gjostein and W.D. Robertson, (ASM, Metals Park, OH, 99 1963).
[6] H.-C. Jeong and E.D. Williams, Surf. Sci. Rep. **34**, 171 (1999).
[7] A. Rettori and J. Villain, J. Phys. (France) **49**, 257 (1988).
[8] M. Ozdemir and A. Zangwill, Phys. Rev. B **42**, 5013 (1990).
[9] N. Israeli and D. Kandel, Phys. Rev. Lett. **80**, 3300 (1998).
[10] N. Israeli and D. Kandel, Phys. Rev. B **60**, 5946 (1999).
[11] H. Spohn, J. Phys. I **3**, 69 (1993).
[12] J. Hager and H. Spohn, Surf. Sci. **324**, 365 (1995).
[13] J.P. Straley and E.B. Kolomeisky (unpublished).
[14] H.P. Bonzel, E. Preuss, and B. Steffen, Appl. Phys. A: Solids Surf. **35**, 1 (1984).
[15] H.P. Bonzel and E. Preuss, Surf. Sci. **336**, 209 (1995).
[16] M.V.R. Murty and B.H. Cooper, Phys. Rev. B **54**, 10 377 (1996).
[17] J.D. Erlebacher and M.J. Aziz, Surf. Sci. **374**, 427 (1997).
[18] P.C. Searson, R. Li, and K. Sieradzki, Phys. Rev. Lett. **74**, 1395 (1995).
[19] W. Selke and P.M. Duxbury, Phys. Rev. B **52**, 17 468 (1995).
[20] W.J. Shugard, J.D. Weeks, and G.H. Gilmer, Phys. Rev. Lett. **41**, 1399 (1978).
[21] S. Tanaka, N.C. Bartelt, C.C. Umbach, R.M. Tromp, and J.M. Blakely, Phys. Rev. Lett. **78**, 3342 (1997).
[22] Note that the real-space amplitude is plotted in Ref. 16 whereas the Fourier amplitude is plotted in Fig. 2.
[23] The same solid-on-solid model shows exponential decay with L^{-4} scaling at $T = 1.13 T_R$. The superposition principle was also satisfied when the decay of two superposed bidirectional sinusoidal profiles of wavelengths $L = 40$ and 80 was compared to the decay with only one wavelength present.
[24] J.Y. Tsao, *Materials Fundamentals of Molecular Beam Epitaxy* (Academic Press, Boston, 1993). Chap. 6.
[25] To see this, consider a hemispherical surface $z = (R^2 - x^2 - y^2)^{1/2}$ and evaluate μ according to Eq. (5) at a point $x = r$, $y = 0$.
[26] R.A. Brain, Ph.D. thesis, California Institute of Technology, 1996.
[27] L.D. Landau and E.M. Lifshitz, *Statistical Physics* (Pergamon Press, Oxford, 1980), p. 520; A.F. Andreev, Sov. Phys. JETP **53**, 1063 (1982).
[28] J. Villain, Europhys. Lett. **2**, 531 (1986)].
[29] Note that the situation is different for a crystal at equilibrium. The probability of a fluctuation in the surface free energy (which depends on the facet radius) away from its equilibrium value goes down exponentially with the deviation from the equilibrium value.
[30] The factors of 1.3 and 0.6 from Eqs. 6.4 and 6.12, respectively, in Sec. 6 of Ref. 7 are also used in estimating β for the bidirectional sinusoidal profile.
[31] P.S. Maiya and J.M. Blakely, J. Appl. Phys. **38**, 698 (1967).
[32] K. Yamashita, H. Bonzel, and H. Ibach, Appl. Phys. **25**, 231 (1981).
[33] M.E. Keeffe, C.C. Umbach, and J.M. Blakely, J. Phys. Chem. Solids **55**, 965 (1994).
[34] That μ must depend on G_1 can be seen by considering the equilibrium shape of a crystal as in Fig. 4 with the additional constraint $z_y = 0$ (relevant to the unidirectional corrugation). For a fixed G_3, μ is a monotonically increasing function of G_1.
[35] J.A. Stroscio, D.T. Pierce, M.D. Stiles, A. Zangwill, and L.M. Sander, Phys. Rev. Lett. **75**, 4246 (1995).
[36] T. Michely and G. Comsa, Nucl. Instrum. Methods Phys. Res. B **82**, 207 (1993).
[37] M.V.R. Murty, T. Curcic, A. Judy, B.H. Cooper, A.R. Woll, J.D. Brock, S. Kycia, and R.L. Headrick, Phys. Rev. Lett. **80**, 4713 (1998).
[38] J.K. Zuo and J.F. Wendelken, Phys. Rev. Lett. **70**, 1662 (1993).
[39] B. Grossmann and P. Peercy, Phys. Rev. Lett. **74**, 4487 (1995).
[40] S.J. Chey, J.E. van Nostrand, and D.G. Cahill, Phys. Rev. Lett. **76**, 3995 (1996).
[41] J. Erlebacher, M.J. Aziz, E. Chason, M.B. Sinclair, and J.A. Floro, Phys. Rev. Lett. **84**, 5800 (2000).
[42] M. Siegert and M. Plischke, Phys. Rev. Lett. **73**, 1517 (1994).